Applied Catalysis B: Environmental 338 (2023) 123025

Contents lists available at ScienceDirect

Applied Catalysis B: Environmental

journal homepage: www.elsevier.com/locate/apcatb

Coordinating the exciton-mediated and carrier-mediated photocatalytic mechanisms of carbon nitride using acetylacetone for enhancing emerging contaminants removal

Qinglun You [a,b], Chunsheng Zhang [a,b], Min Cao [a], Ping Chen [c], Bin Wang [a,b], Yujue Wang [a,b], Jun Huang [a,b], Shubo Deng [a,b], Gang Yu [a,b,d,*]

[a] State Key Joint Laboratory of Environmental Simulation and Pollution Control, School of Environment, Tsinghua University, Beijing 100084, China
[b] Beijing Key Laboratory for Emerging Organic Contaminants Control, Beijing Laboratory for Environmental Frontier Technologies, Beijing 100084, China
[c] School of Environmental Science and Engineering, Guangdong University of Technology, Guangzhou 510006, China
[d] Advanced Interdisciplinary Institute of Environment and Ecology, Beijing Normal University at Zhuhai, Zhuhai 519087, China

ARTICLE INFO

Keywords:
Acetylacetone
Carbon nitride
Co-catalyst
Excitonic effects
Photocatalytic degradation

ABSTRACT

The neglect of exciton-mediated energy and electron transfer mechanisms and the lack of efficient co-catalysts are two essential obstacles to expanding the application of photocatalysis in emerging contaminant treatment. Herein, acetylacetone (AA) was indirectly excited in the visible light region with the assistance of oxygen-doped carbon nitride (OCN) and showed a unique co-catalyst effect through coordinating exciton-mediated and carrier-mediated energy and electron transfer pathways. Specifically, introducing AA enhances the energy transfer efficiency of OCN, promotes reactive oxygen species generation through carrier-mediated and triplet exciton-mediated pathways, and improves exciton-mediated direct energy and electron transfer to diclofenac. As expected, the OCN/AA system showed superior activity for photocatalytic degradation of diclofenac and several other emerging contaminants. Hence, this study offers a ground-breaking viewpoint on the effective co-catalyst effect of AA and an in-depth understanding of how AA coordinates on multiple exciton-mediated and carrier-mediated photocatalytic mechanisms.

1. Introduction

Chemicals that are not currently under regular environmental monitoring and regulation but may enter the environment and pose a known or potential threat to public health and the environment are referred to as “emerging contaminants” [1]. The environmental and health hazards of emerging contaminants have been gradually confirmed through the advancement of environmental monitoring and environmental toxicology, and corresponding control measures are among the major concerns of the scientific community with the anticipated expansion of environmental legislation [2–4]. Developing efficient treatment technology is a crucial regulatory measure to prevent emerging contaminants from releasing and migrating from pollution sources, such as chemical plants, medical institutions, and wastewater treatment plants, and to establish a barrier to human health. At present, photocatalysis is a promising strategy that could generate reactive oxygen species (ROS) and convert macromolecular organic pollutants to nontoxic and harmless products using sunlight as a source of green energy [5]. Substantial research has achieved efficient abatement of various emerging contaminants, including persistent organic pollutants, pharmaceuticals and personal care products, and endocrine disrupting chemicals, and it has demonstrated both economic viability and clean-energy character [6–8].

Nevertheless, despite significant progress, photocatalysis for emerging contaminants control still confronts enormous difficulties. First, it is common to use the carrier-mediated electron transfer and ROS generation processes to explain photocatalytic degradation reactions and even to direct the modification of the photocatalyst for higher carrier separation efficiency; however, this oversimplified theory makes it challenging to accurately reveal the specific or complex photocatalytic mechanism [9,10]. Furthermore, exciton-mediated energy and electron transfer, which has been long ignored, could produce ROS without

* Corresponding author at: State Key Joint Laboratory of Environmental Simulation and Pollution Control, School of Environment, Tsinghua University, Beijing 100084, China.
E-mail address: gangyu@bnu.edu.cn (G. Yu).

https://doi.org/10.1016/j.apcatb.2023.123025
Received 28 March 2023; Received in revised form 9 June 2023; Accepted 20 June 2023
Available online 21 June 2023

carrier separation and offer a catalyst and substrate interaction pathway through regulating the excitonic processes [11]. In brief, rather than relying just on carrier-mediated ROS attacks, it is urgent to coordinate the competitive relationship between excitons and charge carriers and thoroughly investigate the complex interactions of catalyst and reactant under excitonic effects. Second, extensive studies focus on designing or modifying effective photocatalysts, such as graphitic carbon nitride (g-C_3N_4), to get around inherent challenges including quick charge recombination, poor light utilization, and weak redox potential, but universal and/or affordable solutions are still being investigated [12]. Homogeneous molecular co-catalysts provide higher activity without modifying the photocatalyst and the potential for universal activity improvement for pollutant degradation, in contrast. For instance, trifluoroacetic acid acts as a molecular co-catalyst for photocatalytic H_2 evolution through accelerating hole transfer [13]. Additionally, ketones have been proven to be a highly effective co-catalyst for photocatalytic oxygen activation by suppressing nonradiative energy losses and promoting spin transition [14]. Developing such homogeneous molecular co-catalysts, investigating and coordinating the carrier-mediated and exciton-mediated processes, and regulating the interactions of catalyst and reactant for photocatalytic pollutant remediation continue to be quite challenging.

Alternatively, acetylacetone (AA) has prompted significant concern about the remarkable efficiency of the UV/AA process in reducing dyes, pharmaceuticals, and inorganic pollutants and associated mechanisms [15–17]. Exactly, the excited AA under UV irradiation, ^{3}(AA)*, could transfer electrons or energy directly to dyes and pharmaceuticals and also act as a semiquinone radical-like electron shuttle for synchronous arsenite oxidation and nitrate reduction [15–17]. However, without UV radiation, the excited AA and its associated special mechanisms do not exist. Combining AA with visible-light-driven photocatalysts may allow it to be indirectly excited, control carrier-mediated and exciton-mediated processes, and interact with common pollutants even in the visible light region, all of which are crucial but have not yet been reported.

Herein, by taking g-C_3N_4 and a typical emerging contaminant, diclofenac (DCF), as the model system, we demonstrate for the first time that AA could be excited indirectly through oxygen-doped carbon nitride (OCN) under visible light irradiation and act as an efficient co-catalyst for enhancing several emerging contaminants removal. Introducing AA reduces the adverse energy loss of OCN, promotes ROS generation through carrier-mediated electron transfer and triplet exciton-mediated electron and energy transfer, and improves exciton-mediated direct energy and electron transfer to DCF. This study provides a pioneering perspective on the effective co-catalyst effect of AA in the visible light region as well as a thorough explanation of how AA coordinates on multiple exciton-mediated and carrier-mediated energy and electron transfer pathways.

2. Methods and materials

Chemicals and reagents, preparation of photocatalysts, morphology and structure characterization, (photo)electrochemical measurements, and analytic methods of DCF intermediate products are provided in Text S1, S2, S3, S4, and S5 in Supplementary Material.

2.1. Photocatalytic experiments

The degradation of DCF and several other emerging contaminants was conducted in a photochemical reaction system (Fig. S1; PCX-50C Discover, Beijing Perfectlight, China) to assess the photocatalytic performance. The light source for irradiation is a multi-channel lamp panel equipped with 10 W LED lights ($\lambda \geq 420$ nm). Typically, DCF aqueous solution (50 mL, 2 mg/L), photocatalyst (0.04 g/L), and a certain quantity of AA were mixed and stirred for 60 mins before irradiation. The photocatalytic process was continuously stirred and kept at a constant temperature (25.0 ± 0.1°C). The concentration of DCF and AA were detected by high-performance liquid chromatography (HPLC; Shimadzu, Japan) according to previous reports [18,19]. The detailed analytical methods of intermediate products and other emerging contaminants were conveyed in Text S5 and Table S1.

2.2. Electron paramagnetic resonance tests

The generation of different ROS was directly measured using an EMXplus 10/12 electron paramagnetic resonance (EPR) spectrometer (Bruker, Germany). Several spin-trapping agents, including 5,5-dimethyl-1-pyrroline N-oxide (DMPO), 2,2,6,6-tetramethyl-4-piperidone-N (TEMP), and 2,2,6,6-Tetramethyl-1-piperidinyloxy (TEMPO), were used to monitor ·OH, $\cdot O_2^-$, $^1O_2$, and h^+, respectively. In preparation for testing, suspensions containing OCN (1 g/L) and acetylacetone (0 or 25 mM) in water or methanol were illuminated for 1 min using a 300 W xenon lamp (PF300-T8; CEAULIGHT, China). Table S6 lists the spin-trap reagents and solvents of several ROS and h^+/e^- used in EPR studies.

2.3. Optical characterization

The optical absorption spectra were recorded on a UV-2700 UV–vis spectrophotometer (Shimadzu, Japan) in the diffuse reflectance mode. The steady-state photoluminescence (PL) spectra, time-resolved photoluminescence (TR-PL) spectra, phosphorescence spectra (PH), and time-resolved phosphorescence (TR-PH) spectra were collected on a FLS1000 fluorescence spectrometer (Edinburgh, UK). Prior to the measurement of TR-PL, PH, and TRPH, an acetonitrile solution containing acetylacetone (0 or 1 mM) and OCN (0.04 g/L) was swirled and ultrasonically processed. TR-PL and TR-PH were excited at 360 nm and monitored at 488 nm, while TR-PH spectra were obtained at 77K. And more steady-state fluorescence spectra were also recorded using a Hitachi F-7000 fluorescence spectrophotometer (Hitachi, Japan; excited at 360 nm), where OCN (0.04 g/L) and acetylacetone (0, 1, 2, or 3 mM) were dispersed in acetonitrile before measurement.

2.4. Quantum chemistry calculation

The Gaussian 16 software was used for all calculations [20]. For Gibbs free energy change calculations, the basis set 6–31+G(d, p) was used in conjunction with the functional B3LYP for geometry optimization. To confirm that no structure has an imaginary frequency, the harmonic frequency calculations were performed at the same theoretical level. The calculations used the implicit solvation model SMD and water as the solvent. The lowest singlet or triplet excitation energies of AA (E_{S1}/E_{T1}) and the free energy of the ground state of AA were added to obtain the free energy of ^{1}(AA)*/^{3}(AA)* . Open enol, ketone, and chelated enol, three types of AA, were taken into consideration. At the same theoretical level, TD-DFT calculations were used to determine the excitation energies. The M06–2X hybrid functional was used to calculate the energy gaps between the ground state and excited states of AA [21]. The 6–31G(d,p) basis set was employed for geometry optimization. To determine the nature of all the stationary points being the lowest (no imaginary frequency) to obtain the Gibbs free energy adjustments at 298.15K, analytical frequency calculations were carried out at the same theoretical level as the geometry optimization. The lager 6–311+G(d,p) basis set was used to determine the final energies for the structures that had been fully optimized. The nature of their excited states was investigated using the TD-M062X/6–31G(d,p) method.

3. Results and discussion

3.1. Morphology, composition, and structure

Pristine g-C_3N_4 (CN) displays a typical stacked-layered structure in Fig. 1a. And OCN exhibits a distinct structure resembling mitochondria

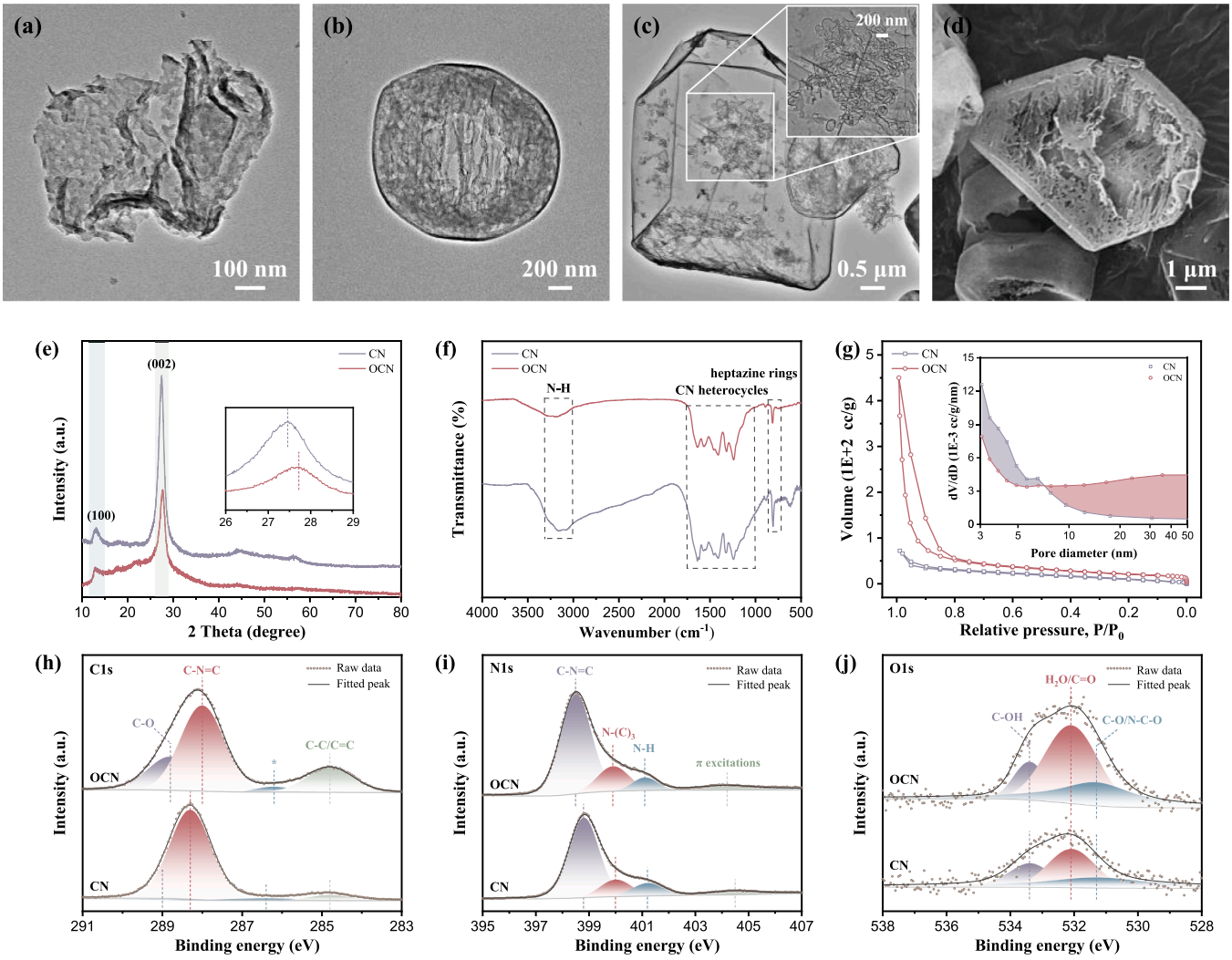

Fig. 1. TEM images of (a) CN and (b-c) OCN. (d) SEM image of OCN. (e) XRD patterns, (f) FT-IR spectra, (g) nitrogen adsorption-desorption isotherms (the pore size distribution curves insert), (h) high-resolution C1s XPS spectra, (i) high-resolution N1s XPS spectra, and (j) high-resolution O1s XPS spectra of CN and OCN.

that encloses a multitude of channels and pores, which would provide more active sites (Fig. 1b-d). In Fig. 1e, X-ray diffraction (XRD) spectroscopy shows that OCN contains two characteristic peaks ((1 0 0) and (0 0 2)) that are similar to but dramatically weaker than those of pure CN. When compared to CN, the characteristic (0 0 2) peak of OCN, ascribed to the interlayer-stacking of conjugated aromatic rings, shifts from 27.46° (d-spacing = 0.3245 nm) to 27.72° (d-spacing = 0.3216 nm), indicating a slight reduction in the interlayer distance and tighter packing of the heptazine system [22]. In Fourier transform infrared spectroscopy (FT-IR, Fig. 1f), OCN obtains the typical vibrations of g-C_3N_4, containing the sharp peak at around 810 cm^{-1}, the multiple peaks from 1000 to 1750 cm^{-1}, and the broad peak from 3000 to 3500 cm^{-1}, indexed to the bending vibration of heptazine rings, the stretching vibrations of CN heterocycles, and the stretching vibration of N−H, respectively [23]. The nitrogen adsorption-desorption isotherm of OCN in Fig. 1g can be differentiated from CN because it has a typical type-IV isotherm featuring a pronounced H1-type hysteresis loop in the region of 0.8–1.0 relative pressure (P/P_0), indicating the existence of mesopore structure. Furthermore, OCN has higher surface areas and remarkable pore volumes, as evidenced by the BET-specific surface area and pore structure as determined using the BET method and BJH method and displayed in Table S2. Elemental analysis measurements, as shown in Table S3, elucidate the abundant O contents in OCN compared with CN. And X-ray photoelectron spectroscopy (XPS) measurements were carried out to further recognize the surface chemical states. Specifically, the high-resolution C1s spectra, N1s spectra, and O1s spectra were deconvoluted and shown in Fig. 1h-j and Table S4. It should be highlighted that OCN has a noticeably greater peak at around 288.9 eV in the C1s spectra, which is linked to C−O/N−C−O (Fig. 1h and Fig. S3b) [24]. Further, the O1s spectrum more convincingly supports the aforementioned findings, demonstrating that O atoms are successfully embedded by substituting N atoms and that OCN may contain numerous oxygen-containing functional groups, such as C−OH, C=O, and COOH [25]. And O atoms might be doped in C−N−C lattice sites, as testified by the lowest formation energy [26].

OCN has similar light adsorption properties to CN, as seen in Fig. 2a, as well as a small blue shift in the light region and the intrinsic absorption edge shift from 474 to 472 nm. And OCN also exhibits decreased light absorption in the UV region (indexed to π→π* electron transition), which might be due to lower crystallinity and deceased periodic structure, namely the conclusion of XRD spectra [27]. According to the Tauc plots, the corresponding bandgaps of CN and OCN were measured to be 2.75 and 2.79 eV, respectively (Fig. 2b). Additionally, the valence band XPS spectra in Fig. 2c demonstrate that the valance band edge potential (E_{VB}) of CN and OCN is 1.93 and 2.13 eV, respectively, meaning that OCN could produce h^+ with a higher

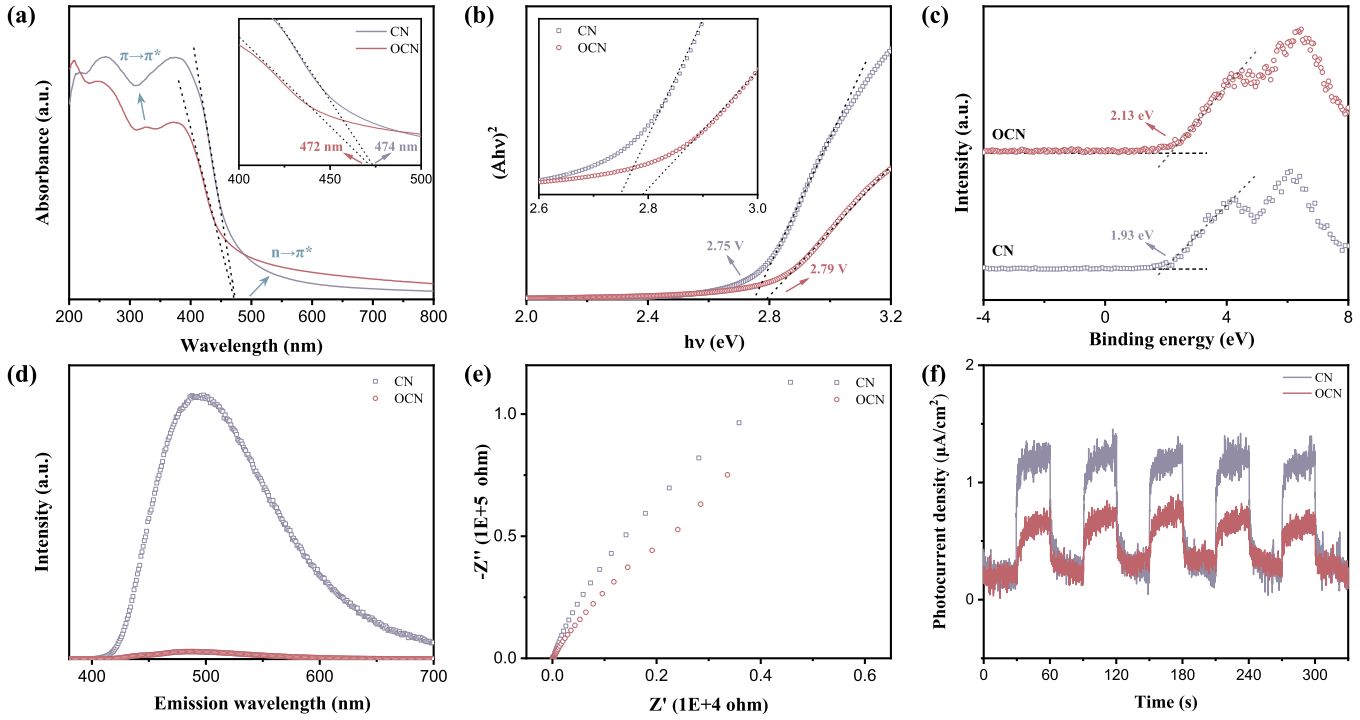

Fig. 2. (a) UV–vis diffuse reflectance spectra (UV-DRS), (b) DRS Tauc plots, (c) valence band XPS spectra, (d) steady-state fluorescence spectra (excited at 360 nm), (e) electrochemical impedance spectra (EIS) Nyquist plots, and (f) the photocurrent responses cycles of CN and OCN.

oxidation capacity. Thereafter, the edge potentials for the conduction band (E_{CB}) were determined and are depicted in Fig. S4. Fig. 2d-e indicate that compared to CN, OCN exhibits a much more quenched photoluminescence signal and a smaller semicircle of the EIS curve, which support less radiative decay of singlet excitons or charge carrier recombination and reduced interface charge transfer resistance [11]. Interestingly, OCN exhibits a lower photocurrent density, which also indicates a poor charge carrier separation. Hence, the decreased PL intensity of OCN may be due to intersystem crossing (ISC) rather than the effect of charge carrier recombination.

Based on the above analyses, OCN, fabricated by the modulation of p-toluenesulfonic acid, has a unique structure resembling the mitochondria, a smaller interlayer distance, rich surface areas and pore volumes, numerous oxygen-containing functional groups, reduced interface charge transfer resistance, and the potential to create h^+ with a higher oxidation capacity.

3.2. Photocatalytic degradation performance

DCF adsorption investigations were conducted in the dark and are shown in Fig. S5a. The adsorption-desorption equilibrium was achieved within 60 mins, and the adsorption could contribute to about 5% DCF removal on OCN. Poor adsorption might be due to the fact that OCN (isoelectric point is about 3.7, Fig. S5b) and DCF (pKa is about 4.1) would have the same charge in the OCN/AA system (pH ≈ 5.5). The photocatalytic degradation experiments were conducted in aqueous solutions upon visible light irradiation, and the data followed the pseudo-first-order kinetic model. As demonstrated in Fig. 3a-b, the degradation of DCF proceeded more quickly with the assistance of OCN with respect to CN, which is due to the aforementioned advantages of OCN. Approximately 19% of DCF was degraded on CN after 150 mins of irradiation, while over 89% of DCF removal was achieved on OCN in the same conditions. It's worth noting that AA alone could not remove DCF under visible light irradiation, but it can effectively promote DCF degradation over CN and OCN. And the kinetic constant (k_{obs}) of the OCN/AA (1 mM) system (k_{obs} = 0.0282 min^{-1}) is about 2, 11, and 26 times higher than that of OCN (k_{obs} = 0.0140 min^{-1}), the CN/AA (1 mM) system (k_{obs} = 0.0026 min^{-1}), and CN (k_{obs} = 0.0011 min^{-1}), respectively. It is crucial to note that AA attenuation in the OCN/AA (1 mM) system is identical to that of AA itself (Fig. S5c), suggesting AA might act as a co-catalyst. According to Fig. 3c-d, the degradation of DCF over OCN improves with the presence of AA, and the rate constants present a bell-shaped pattern as a function of AA content. Anions in water matrixes typically compete for the active site and react with ROS to form less reactive species and thus obstruct the removal of contaminants [28]. However, Fig. 3e-f revealed that concomitant Cl^-, NO_3^-, and SO_4^{2-} have negligible effects on decomposing DCF in the OCN/AA (1 mM) system, while HCO_3^- has minimal impact, indicating the OCN/AA (1 mM) system provided the feasibility for the remediation of contaminants in water and wastewater. As shown in Fig. 3g-i, the propagable co-catalyst effect of AA was validated in numerous emerging contaminants removal. Therein, the degradation of indomethacin (IDM), acetaminophen (ACE), sulfadiazine (SDZ), and ciprofloxacin (CIP) by the OCN/AA (1 mM) system is roughly 5.31, 1.87, 1.76, and 1.37 times faster than that of OCN.

Additionally, under the aforementioned experimental conditions, the energy and chemical agent costs of OCN/AA might also save up to 71% of those of OCN in various presupposed degradation targets, whereas those of CN/AA are 58% to 63% less than those of CN (Table S5 and Figs. S6a-c). Moreover, the OCN/AA system and the CN/AA system demonstrate economic viability. OCN maintains its intact structure after photocatalytic experiments, which suggests a high degree of recyclability, as shown in Figs. S7a-b.

3.3. Photocatalytic degradation mechanism

To determine the type of ROS generated and their effects on DCF decomposition, photocatalytic experiments were carried out in the absence of several scavengers or not. The descending order of the inhibitory effects of scavengers in the OCN/AA (1 mM) system is as shown in Fig. 4a-b: triethanolamine (TEOA, for h^+ quenching) > furfuryl alcohol (FFA, for $^1O_2$ and ·OH quenching) > carbon tetrachloride (CCl_4,

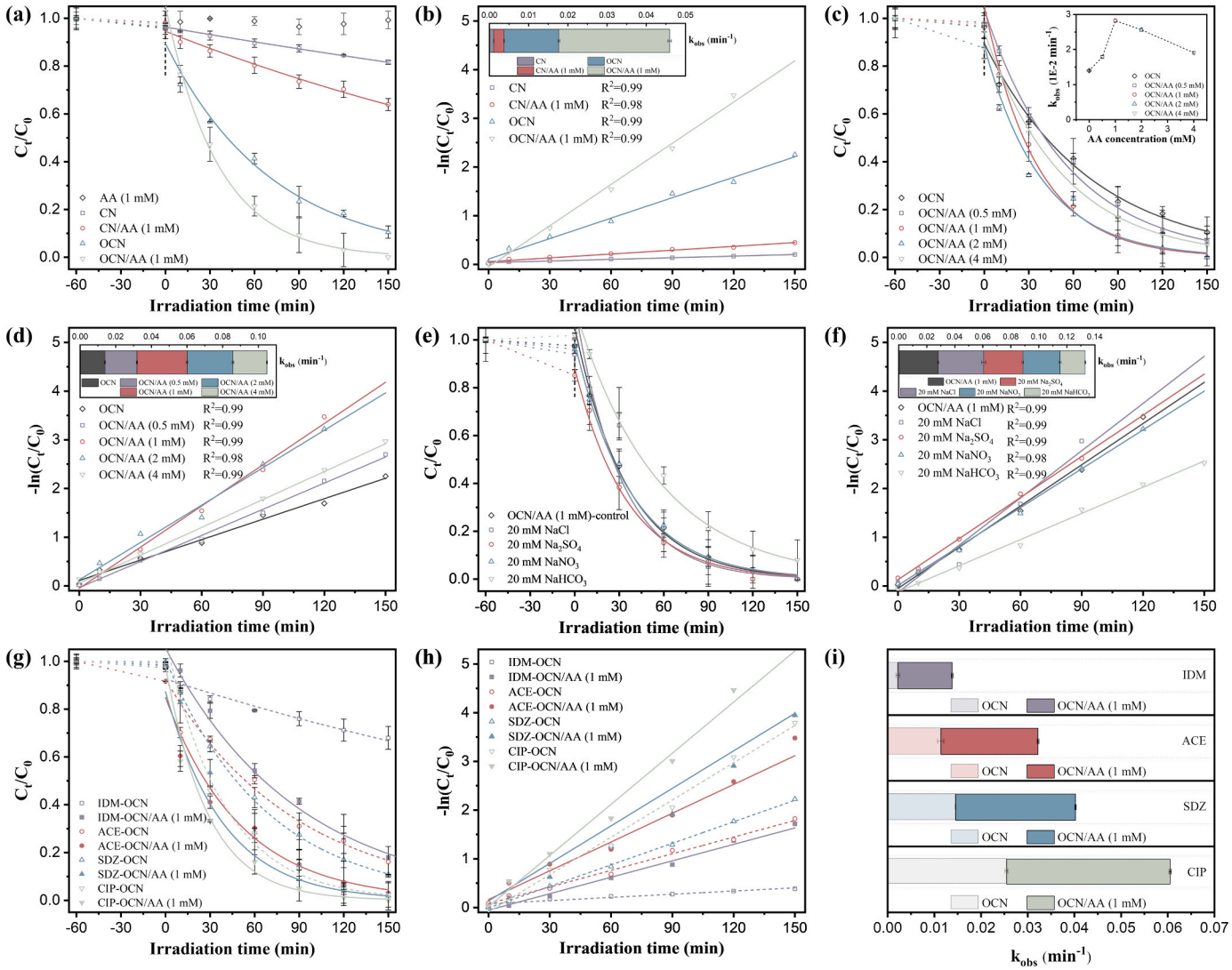

Fig. 3. The kinetic plots, fitted curves, and k_{obs} of the photocatalytic degradation of DCF in different processes. Experimental conditions: The catalytic dose is 0.04 g/L, with $[DCF]_0 = 6.75$ μM (i.e., 2 mg/L), $[IDM]_0 = 5.59$ μM (i.e., 2 mg/L), $[ACE]_0 = 13.23$ μM (i.e., 2 mg/L), $[SDZ]_0 = 7.99$ μM (i.e., 2 mg/L), $[CIP]_0 = 6.04$ μM (i.e., 2 mg/L), $[anions]_0 = 0$ or 20 mM, and $[AA]_0 = 0$, 0.5, 1, 2 or 4 mM.

for $\cdot O_2^-$ quenching) > isopropanol (IPA, for ·OH quenching). Hence, h^+ exhibits the strongest effects in this process, while $\cdot O_2^-$, ·OH, and $^1O_2$ also have significant effects. In contrast, the order in OCN is as shown in Fig. 4c-d: TEOA (for h^+ quenching) >> CCl_4 (for $\cdot O_2^-$ quenching) ≈ FFA (for $^1O_2$ and ·OH quenching) ≈ IPA (for ·OH quenching). Expressly, Fig. 4e demonstrates the comparison of inhibitory effects of different scavengers in OCN and the OCN/AA (1 mM) system. Explicitly, $\cdot O_2^-$, ·OH, and $^1O_2$ are essential species in the OCN/AA (1 mM) system but only slightly contribute to the elimination of DCF over OCN. A significant quenching effect of TEOA indicates the important role of h^+ and may also be partly due to its negative influence on excitons, including disturbing the balance of excitons and carriers and reducing the excitonic lifetime [29]. Electron paramagnetic resonance spectra of OCN and the OCN/AA system were also investigated to further determine the ROS generation and their effects. As illustrated in Figs. S8a-c, no obvious signal was observed prior to irradiation, and OCN displayed the characteristic signals of DMPO-·OH (1:2:2:1), DMPO-$\cdot O_2^-$ (1:1:1:1), and TEMP-$^1O_2$ (1:1:1) adducts, which were further amplified in the presence of AA. Additionally, the triple signals of TEMPO in Fig. S8d were even more suppressed when compared to OCN because more e^- or h^+ were created or separated in the OCN/AA system. Briefly, AA slightly promoted ROS production and h^+/e^- separation on OCN, which is consistent with the scavenger-quenching studies but could not fully explain the high activity of the OCN/AA system.

In recent years, several studies have reported the excitonic energy transfer mechanism in the photocatalytic degradation by g-C_3N_4 under visible light irradiation [30,31]. The scavenger-quenching experiments under anaerobic conditions were also executed to identify possible exciton-mediated photocatalytic mechanisms. Saturated N_2 conditions could exclude the role of ROS in the photocatalytic DCF degradation, and three scavengers further distinguished the effects of triplet exciton, e^-, and h^+. The descending order of the inhibitory effects of scavengers in the OCN/AA (1 mM) system and OCN is as shown in Fig. 4e-i: trimethylphenol (TMP, for triple quenching) > triethanolamine (TEOA, for h^+ quenching) > potassium iodide (KI, for e^- quenching). In particular, TMP shows a significant inhibiting effect on DCF degradation, which demonstrates that the generation of triplet exciton and its energy transfer play a crucial role in the photocatalytic degradation of DCF.

Optical characterization and quantum chemistry calculations were provided for further verification and in-depth exploration of exciton-mediated photocatalytic mechanisms in the OCN/AA system. In comparison to OCN, all tested OCN/AA systems exhibit similar but weaker emission peaks in the steady-state PL spectra, which are usually brought about by the radiative decay of singlet excitons or charge carrier

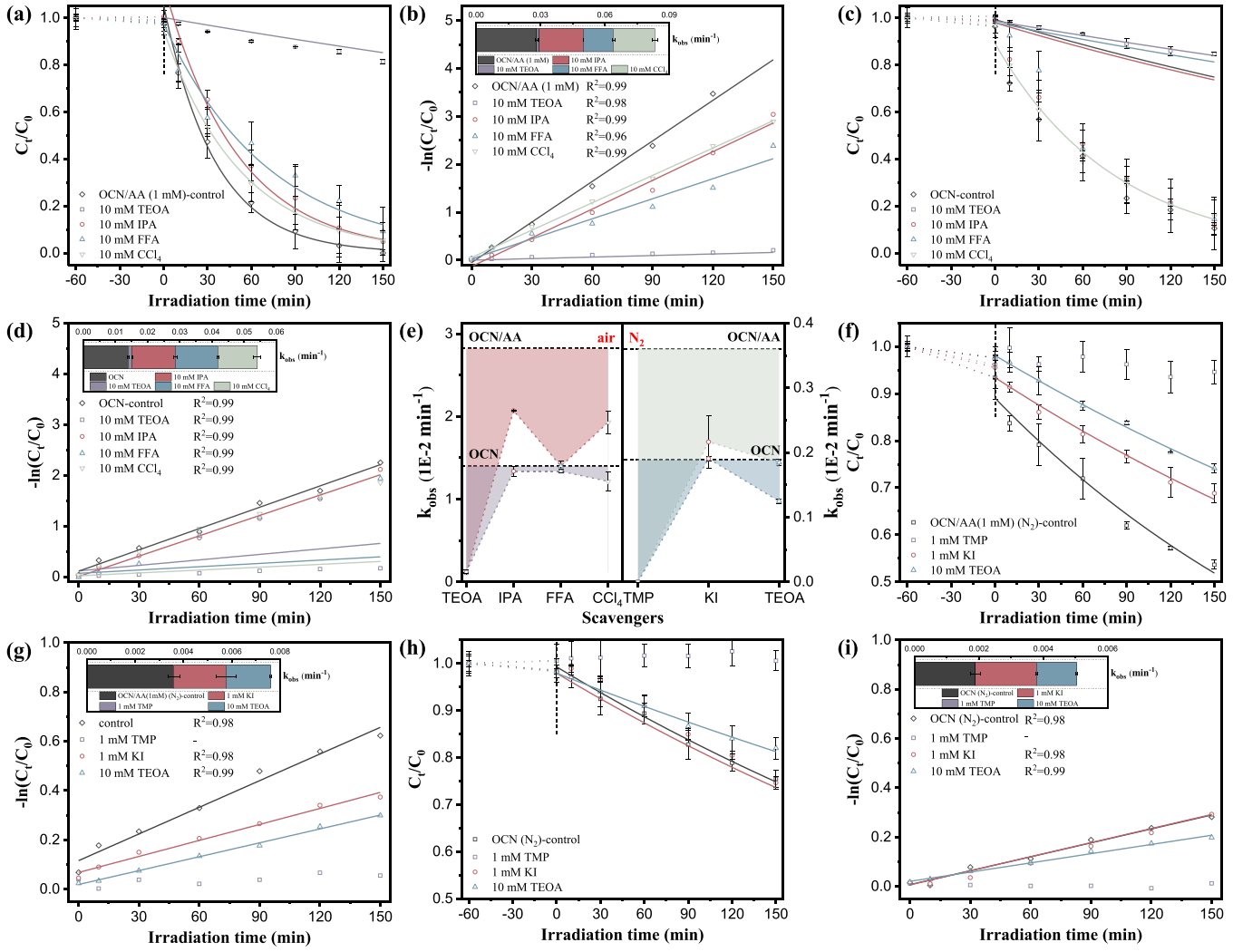

Fig. 4. The kinetic plots, fitted curves, and k_{obs} of the photocatalytic degradation of DCF in different processes. Experimental conditions: The catalytic dose is 0.04 g/L, with $[DCF]_0 = 6.75$ μM (i.e., 2 mg/L), $[AA]_0 = 0$ or 1 mM, and $[scavengers]_0 = 0$, 1 or 10 mM. N_2 denotes experiments with continuous N_2 purging.

recombination [11]. In fact, the steadily decreased PL intensity after adding AA is probably due to enhanced singlet exciton conversion, such as conversion to triplet exciton through ISC, rather than improved charge carrier separation, given the slightly decreased photocurrent density in Fig. 5b [32]. Additionally, a greater triplet exciton yield was observed as a result of the increased phosphorescence (PH) intensity of the OCN/AA system compared to OCN (Fig. 5c) [32,33]. And the increased ΔE_{ST} (the red shift of PH with regard to the PL) (Fig. 5d) further identified the portable presence of other forms of triplet exciton, such as $^3(AA)^*$. And the previously indicated decreased PL intensity was further demonstrated by the fact that the S_1 of AA is in a dark state [34]. The above-mentioned scavenger-quenching experiments under anerobic conditions also indicate that DCF might be excited; however, g-C_3N_4 could not excite AA and DCF through the normal mechanism of photosensitization according to previous studies and calculations (Table S12) [35,36]. Hence, the excitation of AA in the OCN/AA system might be through the energy transfer of exciton–exciton annihilation-induced hot excitons from OCN to AA [14]. And this mechanism would reduce the adverse energy loss of OCN, promote triplet exciton yield, and provide the potential for energy transfer from excited AA to DCF. That supports the indirect excitation of AA by OCN and its conversion to the triplet state under visible-wavelength light irradiation, which was previously unreported. Furthermore, introducing DCF to the OCN/AA system decreased the phosphorescence intensity, and the ΔE_{ST} is between that of OCN and the OCN/AA system, which might be due to the formation of excited DCF and/or the (DCF-AA)* exciplex. The OCN/AA system produced more products with greater mass-to-charge ratios than DCF ($m/z = 350$, 382, 410, and 427) compared to OCN, which might supported the (DCF-AA)* exciplex generated [16]. The calculated Gibbs free energy change (Table S11) further supported the direct electron transfer mechanism between the excited states of AA and DCF [37]. Moreover, the time-resolved photoluminescence (TR-PL) spectra and time-resolved phosphorescence (TR-PH), fitted by the triple-exponential decay function, were also recorded and shown in Fig. 5e-f and Tables S7-8. Coexisting AA and DCF promote the lifetime of phosphorescence decay from 887.42 μs to 973.92 μs and 1432.77 μs, but not photoluminescence decay, signifying more efficient energy transfer.

In light of the prior discoveries and research, we confirm that AA, as a multifunctional co-catalyst, coordinates the exciton-mediated and carrier-mediated electron and energy transfer mechanisms for high-efficiency DCF elimination in the OCN/AA system. Under visible light irradiation, AA could be indirectly excited in the OCN/AA system through extracting the exciton-exciton annihilation-induced hot excitons from OCN, which reduces the adverse energy loss of OCN, promotes the $^3(AA)^*$ generation, and provides the potential for energy transfer from excited AA to DCF. On the one hand, triplet excitons play a role in the energy transfer processes, including more $^1O_2$ formation and the indirect excitation of DCF via energy transfer from excited AA, which

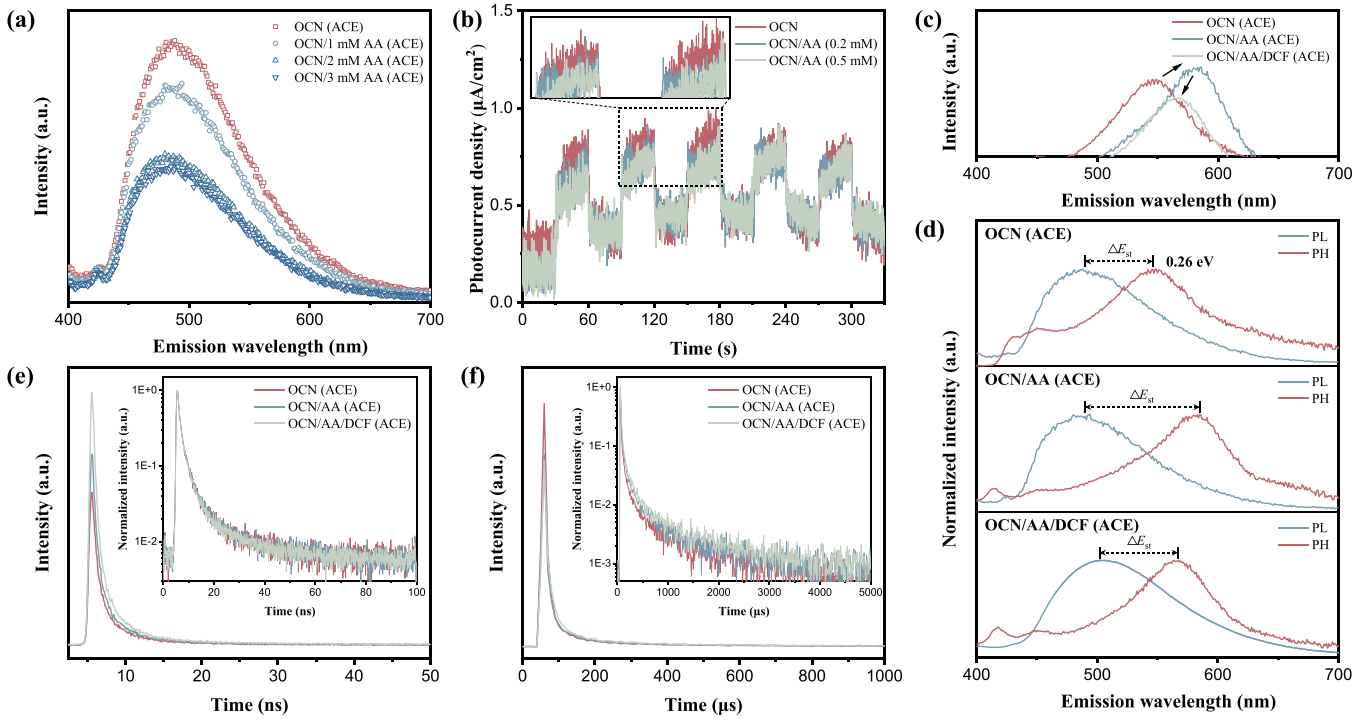

Fig. 5. (a) Steady-state PL spectra (excited at 360 nm), (b) the photocurrent responses cycles of OCN and the OCN/AA system. (c) Steady-state PH spectra of OCN, OCN/AA, and OCN/AA/DCF (excited at 360 nm, delay time: 1 ms). (d) Normalized steady-state PL and PH spectra of OCN, OCN/AA, and OCN/AA/DCF. (e) TR-PL spectra (excited at 360 nm and monitored at 488 nm), (f) TR-PH spectra (excited at 360 nm and recorded at 488 nm at 77K) of OCN, OCN/AA, and OCN/AA/DCF.

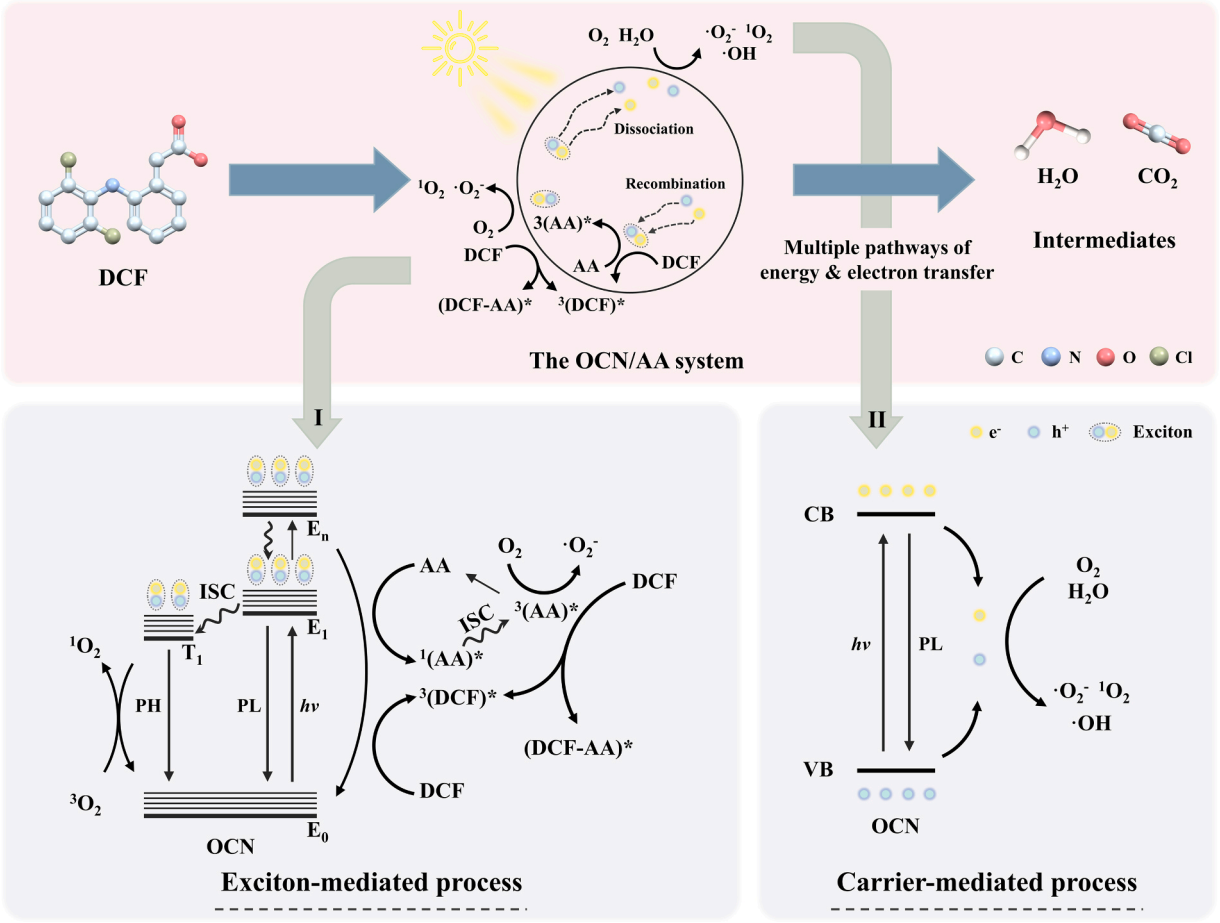

Fig. 6. Proposed photocatalytic DCF degradation mechanism in the OCN/AA system.

leads to the subsequent photolysis of ^{3}(DCF)*. On the other hand, excited AA might combine with DCF to create the (DCF-AA)* exciplex, which is capable of exchanging electrons directly. Furthermore, previous research had demonstrated that the excited state of AA may produce $\cdot O_2^-$ through the electrons transfer to O_2 [37]. Additionally, increasing exciton populations encourage the concentration of charge carriers by exciton dissociation [14]. And separated carriers could directly decompose DCF or other emerging contaminants by h^+ or indirectly by producing $\cdot O_2^-$, $^1O_2$, and ·OH.

4. Conclusion

The neglect of exciton-mediated energy and electron transfer mechanisms and the lack of effective co-catalysts are two essential obstacles to expanding the application of photocatalysis in emerging contaminants treatment. For the first time, this research examined the feasibility of acetylacetone as a molecular co-catalyst for enhancing the photocatalytic degradation of photocatalysts on several emerging contaminants by coordinating the exciton-mediated and carrier-mediated photocatalytic mechanisms.

- The modulation of p-toluenesulfonic acid in self-assembled progress was employed to fabricate oxygen-doped carbon nitride (OCN), which has a unique structure resembling the mitochondria, reduced interlayer distance, abundant surface areas, remarkable pore volume, numerous oxygen-containing functional groups, lower interface charge transfer resistance, and the potential to create h^+ with a higher oxidation capacity.
- With the assistance of OCN, AA could be indirectly excited under visible light irradiation, increasing the long-lived exciton yield and energy transfer efficiency. Excited AA could excite DCF through the energy transfer. Correspondingly, more $^1O_2$ and $\cdot O_2^-$ form through the energy transfer of exciton and the electron transfer from the excited state of AA, and the (DCF-AA)* exciplex that is capable of exchanging electrons directly generates. Meanwhile, increasing exciton populations encourage the concentration of charge carriers and the corresponding ROS formation.
- The OCN/AA system showed superior activity for the photocatalytic degradation of several emerging contaminants (DCF, IDM, ACE, SDZ, and CIP). Particularly, the OCN/AA system exhibits 26 times higher activity than that of CN, superior anti-interference performance for concomitant anions, low AA consumption, recyclability of OCN, and sound economic viability.

Overall, this study offers a ground-breaking viewpoint for the effective co-catalyst effect of AA in the visible light region as well as an in-depth understanding of the coordination of AA on the exciton-mediated and carrier-mediated energy and electron transfer pathways. The OCN/AA system holds potential as a proof-of-theory, and further research is required to confirm the general applicability of AA's co-catalysis in photocatalytic water remediation in real-world conditions.

CRediT authorship contribution statement

Qinglun You: Conceptualization, Methodology, Investigation, Data curation, Visualization, Writing - original draft, Writing - review & editing. **Chunsheng Zhang**: Investigation, Data curation. **Min Cao**: Investigation, Data curation, Software. **Ping Chen**: Conceptualization, Methodology. **Bin Wang**: Resources, Funding acquisition. **Yujue Wang**: Resources, Funding acquisition. **Jun Huang**: Resources, Funding acquisition. **Shubo Deng**: Resources, Funding acquisition. **Gang Yu**: Resources, Writing - review & editing, Funding acquisition.

Declaration of Competing Interest

The authors declare that they have no known competing financial interests or personal relationships that could have appeared to influence the work reported in this paper.

Data Availability

Data will be made available on request.

Acknowledgment

This work was financially supported by the Major Science and Technology Program for Water Pollution Control and Treatment in China (2017ZX07202006).

Appendix A. Supporting information

Supplementary data associated with this article can be found in the online version at doi:10.1016/j.apcatb.2023.123025.

References

[1] S.D. Richardson, Emerging contaminants: The need for elegant analytical chemistry solutions for the new environmental pollutants of concern, Abstr. Pap. Am. Chem. Soc. 222 (2001). U431-U431.
[2] D.J. Lapworth, N. Baran, M.E. Stuart, R.S. Ward, Emerging organic contaminants in groundwater: a review of sources, fate and occurrence, Environ. Pollut. 163 (2012) 287–303.
[3] M. Cleuvers, Aquatic ecotoxicity of pharmaceuticals including the assessment of combination effects, Toxicol. Lett. 142 (2003) 185–194.
[4] B. Petrie, R. Barden, B. Kasprzyk-Hordern, A review on emerging contaminants in wastewaters and the environment: Current knowledge, understudied areas and recommendations for future monitoring, Water Res. 72 (2015) 3–27.
[5] X. Chen, S.S. Mao, Titanium dioxide nanomaterials: synthesis, properties, modifications, and applications, Chem. Rev. 107 (2007) 2891–2959.
[6] H. Dong, G. Zeng, L. Tang, C. Fan, C. Zhang, X. He, Y. He, An overview on limitations of TiO_2-based particles for photocatalytic degradation of organic pollutants and the corresponding countermeasures, Water Res. 79 (2015) 128–146.
[7] Y. Hou, F. Liu, B. Zhang, M. Tong, Thiadiazole-based covalent organic frameworks with a donor-acceptor structure: Modulating intermolecular charge transfer for efficient photocatalytic degradation of typical emerging contaminants, Environ. Sci. Technol. 56 (2022) 16303–16314.
[8] H.M. Coleman, K. Chiang, R. Amal, Effects of Ag and Pt on photocatalytic degradation of endocrine disrupting chemicals in water, Chem. Eng. J. 113 (2005) 65–72.
[9] H. Wang, D. Yong, S. Chen, S. Jiang, X. Zhang, W. Shao, Q. Zhang, W. Yan, B. Pan, Y. Xie, Oxygen-vacancy-mediated exciton dissociation in BiOBr for boosting charge-carrier-involved molecular oxygen activation, J. Am. Chem. Soc. 140 (2018) 1760–1766.
[10] Y. Li, S. Jin, X. Xu, H. Wang, X. Zhang, Excitonic effects on photophysical processes of polymeric carbon nitride, J. Appl. Phys. 127 (2020).
[11] D. Zhang, P. Wang, J. Wang, Y. Li, Y. Xia, S. Zhan, Tailoring of electronic and surface structures boosts exciton-triggering photocatalysis for singlet oxygen generation, Proc. Natl. Acad. Sci. 118 (2021).
[12] W. Zhang, A.R. Mohamed, W.J. Ong, Z-scheme photocatalytic systems for carbon dioxide reduction: Where are we now? Angew. Chem. 59 (2020) 22894–22915.
[13] W. Bi, X. Li, L. Zhang, T. Jin, L. Zhang, Q. Zhang, Y. Luo, C. Wu, Y. Xie, Molecular co-catalyst accelerating hole transfer for enhanced photocatalytic H_2 evolution, Nat. Commun. 6 (2015) 8647.
[14] H. Wang, S. Jiang, W. Liu, X. Zhang, Q. Zhang, Y. Luo, Y. Xie, Ketones as molecular co-catalysts for boosting exciton-based photocatalytic molecular oxygen activation, Angew. Chem. 59 (2020) 11093–11100.
[15] Z. Chen, X. Song, S. Zhang, B. Wu, G. Zhang, B. Pan, Acetylacetone as an efficient electron shuttle for concerted redox conversion of arsenite and nitrate in the opposite direction, Water Res. 124 (2017) 331–340.
[16] G. Zhang, B. Wu, S. Zhang, Effects of acetylacetone on the photoconversion of pharmaceuticals in natural and pure waters, Environ. Pollut. 225 (2017) 691–699.
[17] B. Wu, G. Zhang, S. Zhang, Fate and implication of acetylacetone in photochemical processes for water treatment, Water Res. 101 (2016) 233–240.
[18] Q. You, Q. Zhang, M. Gu, R. Du, P. Chen, J. Huang, Y. Wang, S. Deng, G. Yu, Self-assembled graphitic carbon nitride regulated by carbon quantum dots with optimized electronic band structure for enhanced photocatalytic degradation of diclofenac, Chem. Eng. J. 431 (2022), 133927.
[19] B. Wu, S. Zhang, X. Li, X. Liu, B. Pan, Iron in non-hydroxyl radical mediated photochemical processes for dye degradation: Catalyst or inhibitor? Chemosphere 131 (2015) 55–62.
[20] M.J.T. Frisch, G.W.; Schlegel, H. B.; Scuseria, G. E.; Robb, M. A.; Cheeseman, J. R.; Scalmani, G.; Barone, V.; Petersson, G. A.; Nakatsuji, H.; Li, X.; Caricato, M.; Marenich, A. V.; Bloino, J.; Janesko, B. G.; Gomperts, R.; Mennucci, B.; Hratchian, H. P.; Ortiz, J. V.; Izmaylov, A. F.; Sonnenberg, J. L.; Williams; Ding, F.; Lipparini, F.; Egidi, F.; Goings, J.; Peng, B.; Petrone, A.; Henderson, T.; Ranasinghe, D.; Zakrzewski, V. G.; Gao, J.; Rega, N.; Zheng, G.; Liang, W.; Hada, M.; Ehara, M.;

Toyota, K.; Fukuda, R.; Hasegawa, J.; Ishida, M.; Nakajima, T.; Honda, Y.; Kitao, O.; Nakai, H.; Vreven, T.; Throssell, K.; Montgomery Jr., J. A.; Peralta, J. E.; Ogliaro, F.; Bearpark, M. J.; Heyd, J. J.; Brothers, E. N.; Kudin, K. N.; Staroverov, V. N.; Keith, T. A.; Kobayashi, R.; Normand, J.; Raghavachari, K.; Rendell, A. P.; Burant, J. C.; Iyengar, S. S.; Tomasi, J.; Cossi, M.; Millam, J. M.; Klene, M.; Adamo, C.; Cammi, R.; Ochterski, J. W.; Martin, R. L.; Morokuma, K.; Farkas, O.; Foresman, J. B.; Fox, D. J., Gaussian 16, revision A. 03, Wallingford, CT, 2016.

[21] Y. Zhao, D.G. Truhlar, The M06 suite of density functionals for main group thermochemistry, thermochemical kinetics, noncovalent interactions, excited states, and transition elements: two new functionals and systematic testing of four M06-class functionals and 12 other functionals, Theor. Chem. Acc. 120 (2008) 215–241.

[22] C.I. Sathish, S. Premkumar, X. Chu, X. Yu, M.B.H. Breese, M. Al-Abri, A.H. Al-Muhtaseb, A. Karakoti, J. Yi, A. Vinu, Microporous carbon nitride ($C_3N_{5.4}$) with tetrazine based molecular structure for efficient adsorption of CO_2 and water, Angew. Chem. 60 (2021) 21242–21249.

[23] J. Fu, B. Zhu, C. Jiang, B. Cheng, W. You, J. Yu, Hierarchical porous O-doped g-C_3N_4 with enhanced photocatalytic CO_2 reduction activity, Small 13 (2017).

[24] S. Samanta, R. Yadav, A. Kumar, A. Kumar Sinha, R. Srivastava, Surface modified C, O co-doped polymeric g-C_3N_4 as an efficient photocatalyst for visible light assisted CO_2 reduction and H_2O_2 production, Appl. Catal. B 259 (2019), 118054.

[25] Q. You, C. Zhang, M. Cao, B. Wang, J. Huang, Y. Wang, S. Deng, G. Yu, Defects controlling, elements doping, and crystallinity improving triple-strategy modified carbon nitride for efficient photocatalytic diclofenac degradation and H_2O_2 production, Appl. Catal. B 321 (2023), 121941.

[26] Z.-F. Huang, J. Song, L. Pan, Z. Wang, X. Zhang, J.-J. Zou, W. Mi, X. Zhang, L. Wang, Carbon nitride with simultaneous porous network and O-doping for efficient solar-energy-driven hydrogen evolution, Nano Energy 12 (2015) 646–656.

[27] G. Zhang, G. Li, Z.A. Lan, L. Lin, A. Savateev, T. Heil, S. Zafeiratos, X. Wang, M. Antonietti, Optimizing optical absorption, exciton dissociation, and charge transfer of a polymeric carbon nitride with ultrahigh solar hydrogen production activity, Angew. Chem. 56 (2017) 13445–13449.

[28] Y. Zou, W. Wang, H. Wang, C. Pan, J. Xu, I.P. Pozdnyakov, F. Wu, J. Li, Interaction between graphene oxide and acetaminophen in water under simulated sunlight: Implications for environmental photochemistry of PPCPs, Water Res. 228 (2023), 119364.

[29] H. Wang, S. Jin, X. Zhang, Y. Xie, Excitonic effects in polymeric photocatalysts, Angew. Chem. 59 (2020) 22828–22839.

[30] P. Gan, Y. Lu, Y. Li, W. Liu, L. Chen, M. Tong, J. Liang, Non-radical degradation of organic pharmaceuticals by g-C_3N_4 under visible light irradiation: The overlooked role of excitonic energy transfer, J. Hazard. Mater. 445 (2023), 130549.

[31] J. Liang, W. Zhang, Z. Zhao, W. Liu, J. Ye, M. Tong, Y. Li, Different degradation mechanisms of carbamazepine and diclofenac by single-atom Barium embedded g-C_3N_4: the role of photosensitation-like mechanism, J. Hazard. Mater. 416 (2021), 125936.

[32] Z. Zeng, Y. Fan, X. Quan, H. Yu, S. Chen, S. Zhang, Energy-transfer-mediated oxygen activation in carbonyl functionalized carbon nitride nanosheets for high-efficient photocatalytic water disinfection and organic pollutants degradation, Water Res. 177 (2020), 115798.

[33] R. Zhang, Y. Liu, Z. Wang, P. Wang, Z. Zheng, X. Qin, X. Zhang, Y. Dai, M.-H. Whangbo, B. Huang, Selective photocatalytic conversion of alcohol to aldehydes by singlet oxygen over Bi-based metal-organic frameworks under UV–vis light irradiation, Appl. Catal. B 254 (2019) 463–470.

[34] P.K. Verma, F. Koch, A. Steinbacher, P. Nuernberger, T. Brixner, Ultrafast UV-induced photoisomerization of intramolecularly H-bonded symmetric β-diketones, J. Am. Chem. Soc. 136 (2014) 14981–14989.

[35] T. Yuan, F. Yuan, X. Li, Y. Li, L. Fan, S. Yang, Fluorescence-phosphorescence dual emissive carbon nitride quantum dots show 25% white emission efficiency enabling single-component WLEDs, Chem. Sci. 10 (2019) 9801–9806.

[36] R.J. Squibb, M. Sapunar, A. Ponzi, R. Richter, A. Kivimäki, O. Plekan, P. Finetti, N. Sisourat, V. Zhaunerchyk, T. Marchenko, L. Journel, R. Guillemin, R. Cucini, M. Coreno, C. Grazioli, M. Di Fraia, C. Callegari, K.C. Prince, P. Decleva, M. Simon, J.H.D. Eland, N. Došlić, R. Feifel, M.N. Piancastelli, Acetylacetone photodynamics at a seeded free-electron laser, Nat. Commun. 9 (2018) 63.

[37] G. Zhang, M. Xie, J. Zhao, S. Wei, H. Zheng, S. Zhang, Key structural features that determine the selectivity of UV/acetylacetone for the degradation of aromatic pollutants when compared to UV/H_2O_2, Water Res. 196 (2021), 117046.